DE-FG02-84ER13183
Fundamental Studies of the Reforming of Oxygenated Compounds over Supported Metal Catalysts

James A. Dumesic, PI
University of Wisconsin – Madison

The Board of Regents of the University of Wisconsin System
University of Wisconsin – Madison
Research and Sponsored Programs
21 North Park Street, Suite 6401
Madison, WI 53715-1218

Dr. James A. Dumesic
Vilas Research Professor
Michel Boudart Professor of Chemical and Biological Engineering
University of Wisconsin – Madison
College of Engineering
Department of Chemical and Biological Engineering
3014 Engineering Hall
1415 Engineering Drive
Madison, WI 53706-1607
(608) 262-1095
jdumesic@wisc.edu

Executive Summary:

The main objective of our research has been to elucidate fundamental concepts associated with controlling the activity, selectivity, and stability of bifunctional, metal-based heterogeneous catalysts for tandem reactions, such as liquid-phase conversion of oxygenated hydrocarbons derived from biomass. We have shown that bimetallic catalysts that combine a highly-reducible metal (e.g., platinum) with an oxygen-containing metal promoter (e.g., molybdenum) are promising materials for conversion of oxygenated hydrocarbons because of their high activity for selective cleavage for carbon-oxygen bonds. We have developed methods to stabilize metal nanoparticles against leaching and sintering under liquid-phase reaction conditions by using atomic layer deposition (ALD) to apply oxide overcoat layers. We have used controlled surface reactions to produce bimetallic catalysts with controlled particle size and controlled composition, with an important application being the selective conversion of biomass-derived molecules. The synthesis of catalysts by traditional methods may produce a wide distribution of metal particle sizes and compositions; and thus, results from spectroscopic and reactions kinetics measurements have contributions from a distribution of active sites, making it difficult to assess how the size and composition of the metal particles affect the nature of the surface, the active sites, and the catalytic behavior. Thus, we have developed methods to synthesize bimetallic nanoparticles with controlled particle size and controlled composition to achieve an effective link between characterization and reactivity, and between theory and experiment. We have also used ALD to modify supported metal catalysts by addition of promoters with atomic-level precision, to

produce new bifunctional sites for selective catalytic transformations. We have used a variety of techniques to characterize the metal nanoparticles in our catalysts, including scanning transmission electron microcopy (STEM) to measure size and structure, energy dispersive X-ray spectroscopy (EDS) to measure atomic composition, X-ray absorption spectroscopy (XAS) to measure oxidation state and metal coordination, Fourier transform infrared spectroscopy (FTIR) to study adsorbed species, laser Raman spectroscopy to probe metal oxide promoters, and temperature programmed reaction/desorption to study the energetics of adsorption and desorption processes. We have studied our bimetallic catalysts for the selective cleavage of carbon-oxygen bonds, and we have studied the effects of adding metal oxide promoters to supported platinum and gold catalysts for water-gas shift (i.e., the production of hydrogen by reaction of carbon monoxide with water). We anticipate that the knowledge obtained from our studies will allow us to identify promising directions for new catalysts that show high activity, selectivity, and stability for important reactions, such as the conversion of biomass-derived oxygenated hydrocarbons to fuels and chemicals.

Project Objectives:

The main objective of our proposed research was to elucidate the fundamental concepts associated with controlling the activity, selectivity, and stability of bifunctional, metal-based heterogeneous catalysts for tandem reactions, such as liquid-phase conversion of oxygenated hydrocarbons derived from biomass. We have shown that bimetallic catalysts that combine a highly-reducible metal (e.g., Pt, Rh) with an oxophilic promoter (e.g. Re) are promising materials for conversion of oxygenated hydrocarbons because of their high activity and selectivity for C-O scission reactions. These reactions are bifunctional in nature, where the highly-reducible metal catalyzes hydrogenation reactions and the oxophilic promoter facilitates acid-catalyzed reactions. In our future work, we plan to characterize and understand the active sites of such catalysts, focusing initially on the Rh-Re, Rh-Mo, and Pt-Mo systems. In this research, we synthesized nanoparticles with well-controlled and defined particle size and composition by means of controlled surface reactions. The catalyst synthesis starts with a supported Rh or Pt catalyst, and it involves the selective adsorption and reaction on the reduced metal surface of cyclopentadienyl rhenium tricarbonyl ($(C_5H_5)Re(CO)_3$) or cycloheptatriene molybdenum tricarbonyl ($(C_7H_8)Mo(CO)_3$) in a N_2 atmosphere, followed by temperature programmed reduction in H_2 to achieve alloy formation. We used scanning transmission electron microcopy (STEM) and energy dispersive X-ray spectroscopy (EDS) to determine the metal particle size and composition distributions of individual nanoparticles, and we compared the average composition of the nanoparticles measured by STEM/EDS with the bulk composition measured by inductively coupled plasma – atomic emission spectroscopy (ICP-AES). In addition, we employed in situ XAS to probe the coordination environment of the oxophilic promoter (Mo) and the reducible catalytic metal (Pt). We carried out reaction kinetics measurements (e.g., selective hydrogenolysis of 2-hydroxymethyl)tetrahydropyran to elucidate the effect of the bimetallic composition on catalytic activity.

Another objective of our research was to stabilize supported metal catalysts against leaching and sintering during liquid-phase reaction conditions employed during biomass conversion reactions. Precious metal catalysts are used extensively in the petrochemical industry and are anticipated to have a significant role in future biorefineries. While it would be desirable to replace precious metal catalysts (e.g., Pt) with base metals that are more earth-abundant (e.g., Cu), base metal catalysts are susceptible to irreversible deactivation through sintering and/or

leaching under liquid-phase conditions. Irreversible deactivation of a catalyst is a significant impediment for a practical catalytic process, as replacement of a deactivated catalyst can be expensive, require lengthy process shutdowns, and create solid waste that requires reprocessing. Additionally, capital costs associated with precious metal catalysts pose significant barriers to the economic viability of new processes. Accordingly, the search for base-metal catalysts that are stable under liquid-phase reaction conditions remains an important challenge in the field of heterogeneous catalysis.

In this project, we successfully developed a method to stabilize copper nanoparticles supported on γ-Al_2O_3 by atomic layer deposition (ALD) of an alumina overcoat. While ALD has been shown to inhibit nanoparticle mobility of precious metal catalysts under gas-phase conditions, we reported for the first time that ALD can stabilize a base-metal catalyst for liquid-phase catalytic processing. Combining reaction kinetic studies, advanced materials characterization, and first principles calculations we elucidate how the overcoat provides stability to the nanoparticles without appreciably affecting the reaction kinetics. In these studies, we employed XAS, scanning tunneling microscopy (STM), and FTIR measurements of adsorbed probe molecules (e.g., CO). A key part of this research was the use of high resolution STEM studies to quantify morphologies and spatial distributions of ALD overlayers on model catalysts using non-porous silica nanospheres as catalyst supports. We also explored modification of the overcoating material to introduce bifunctionality to the catalyst, for example, by overcoating with a mixed oxide phase such as NbO_x/AlO_x to impart acidity. This ALD approach is complementary to the aforementioned controlled synthesis approach in that the goal of both approaches is to modify supported metal catalysts by addition of promoters with atomic-level precision, to produce new bifunctional sites for selective catalytic transformations.

We anticipate that the knowledge obtained from our studies will allow us to identify promising directions for new catalysts that show high activity, selectivity, and stability for important reactions, such as the conversion of biomass-derived oxygenated hydrocarbons to fuels and chemicals.

Project Activities:

1. **Introduction**

Our work funded by DOE has focused on fundamental challenges commonly encountered in heterogeneous catalysis that are especially important for the conversion of biomass-derived oxygenates: activity, selectivity and catalyst stability. An important challenge is the issue of catalyst selectivity. The presence of multiple functional groups provides for various reaction pathways that can lead to low overall yield of the desired final product. Bifunctional catalysts that combine a highly-reducible metal (e.g., Pt, Rh) with an oxophilic promoter (e.g., Re) have shown promise as selective catalysts for oxygenated reactants because of their high activity and selectivity for C-O scission reactions. Our work has focused on elucidating the nature of the active sites for these unique catalysts.

A second challenge is the issue of catalyst stability and recyclability. It would be highly desirable to replace precious metals (e.g., Pt) with base metals that are more earth abundant (e.g., Cu); however, base metals are more susceptible to irreversible deactivation through sintering and leaching, especially in the liquid-phase conditions common in the processing of biomass-derived oxygenates. In this respect, we have developed a method to stabilize copper nanoparticles supported on γ-Al_2O_3 by ALD of an alumina overcoat.

2. Recent Work

2.1 Bifunctional RhRe/C catalysts for C-O hydrogenolysis

We have shown that the combination of an oxophilic promoter with a highly-reducible metal results in the formation of a bifunctional catalyst that possesses both acid and metal sites.[1] We demonstrated this concept with experimental studies and first-principle density functional theory (DFT) calculations (in collaboration with Robert Davis and Matt Neurock), where the reactivity trends over the RhRe/C catalyst were consistent with C-O hydrogenolysis proceeding through initial acid-catalyzed ring-opening or dehydration followed by metal-catalyzed hydrogenation.[1] The apparent Brønsted acidity of this catalyst was proposed to arise from the deprotonation of hydroxyl groups on rhenium atoms associated with rhodium. (Table 1)

We have shown that the reduction temperature for a RhRe/C catalyst (molar ratio Rh:Re = 1:0.5) prior to exposure to continuous-flow reaction conditions has a significant effect on the activity for the conversion of 2-hydroxymethyltetrahydropyran (HMTHP) to 1,6-hexanediol (1,6-HDO) (Figure 1), which correlates with the change in the number of active sites quantified by NH_3–TPD (Table 1). Additionally, we studied this catalyst for an acid-catalyzed reaction important in biomass conversion processes: the dehydration of fructose to 5-hydroxymethylfurfural (HMF) (Figure 1).[2-5] We also investigated the nature of the active sites on RhRe/C catalyst using XAS under *in situ* and *operando* conditions (in collaboration with Fabio Ribeiro at Purdue and Jeff Miller at Argonne National Laboratory) to probe the relationship between catalyst structure and activity.

Table 1| Effect of reduction temperature on NH_3-titrated site density and activity for hydrogenolysis of HMTHP to 1,6-HDO over RhRe/C under continuous flow conditions.[a]

Catalyst	Pretreatment T (K)	Irreversible CO uptake ($\mu mol g^{-1}$)	Total NH_3 site density ($\mu mol g^{-1}$)	Conversion (%)	Selectivity to 1,6-HDO (%)	Specific rate at 8h TOS ($\mu mol g^{-1} min^{-1}$)
RhRe/C	393	143	95	9	90	56
	523	145	64	9	96	29
	723	135	38	10	95	7
Rh/C	523		30			
Re/C	523		17			

[a]Reaction conditions described in Figure 2.

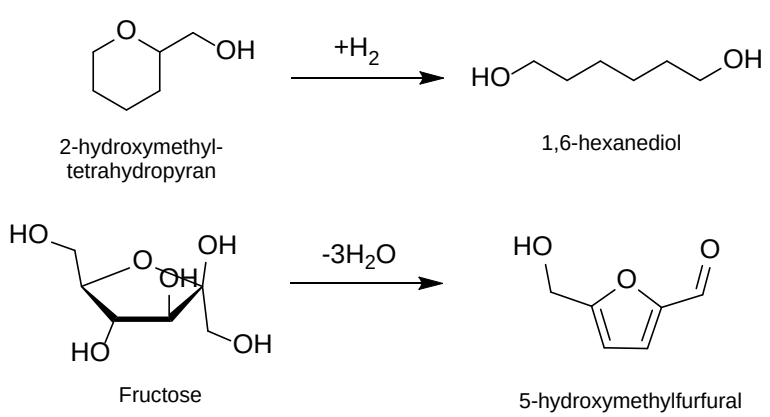

Figure 1| Reactions discussed in this section: C-O hydrogenolysis of HMTHP to 1,6-HDO, and dehydration of fructose to HMF.

The effect of reduction temperature on the catalytic activity for C-O hydrogenolysis of cyclic ethers[6] was investigated under continuous-flow reaction conditions using RhRe/C pretreated in hydrogen at 393, 523, and 723 K. As shown in Figure 2, the rate of C-O hydrogenolysis of HMTHP decreased with increasing pretreatment temperature. The selectivity to 1,6-HDO was maintained at >90% for all data points. It was found that deactivation of the catalyst pretreated at 393 K was significant, while catalysts pretreated at 523 and 723 K were stable. The deactivation of the catalyst pretreated at 393 K is due to leaching of Re species from the surface of the RhRe/C catalyst.

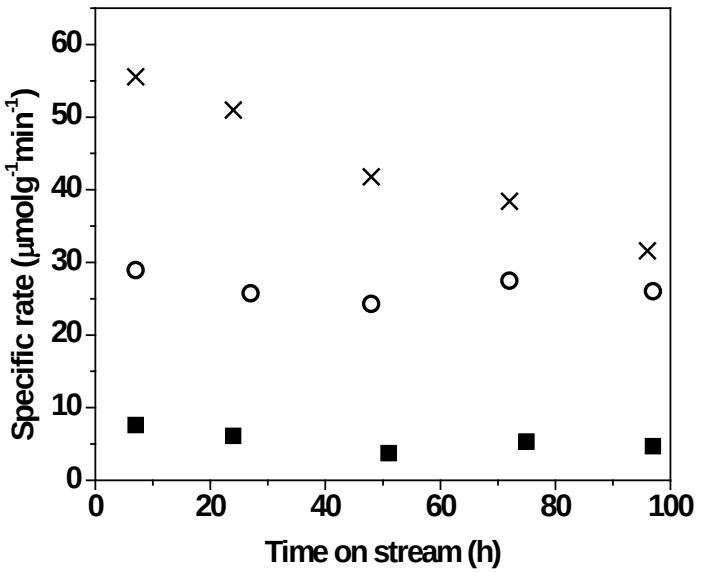

Figure 2| Hydrogenolysis of HMTHP over RhRe/C under continuous flow reaction conditions. Catalyst pretreated in flowing H_2 at 393 K (×), 523 K (○) and 723 K (■) prior to initiation of liquid feed. Selectivities to 1,6-HDO were >90% for all data points. Reaction conditions: 5 wt% HMTHP in water as feed, 393 K, 34 bar H_2.

XAS was used to obtain insight into the structure of the RhRe/C catalyst after pretreatment and under C-O hydrogenolysis conditions. High-angle annular dark-field-scanning transmission electron microscopy (HAADF-STEM) analysis of the catalyst (in collaboration with Abhaya Datye at University of New Mexico) was used to support the conclusions from XAS. The HAADF-STEM results show that the number-averaged particle size was 2.13 ± 0.65 nm (n = 800 particles).[1] This particle size corresponds to bimetallic particles with average EXAFS coordination numbers in the range of 6-8. Additionally, EDS spot-beam analysis of individual particles indicated the presence of both Rh and Re.[1] X-ray absorption spectra for the Rh K-edge and the Re L_{III}-edge were obtained for Rh/C, Re/C, and RhRe/C at room temperature in He after pretreatment in flowing H_2 at 298 to 723 K, which is denoted as *in situ* conditions. Spectra at the Rh K and Re L_{III}-edges for the RhRe/C catalyst were also measured after pretreatment in flowing H_2 at 523 and 723 K and under continuous flow C-O hydrogenolysis reaction conditions (i.e., 34 bar H_2, 393 K, 5 wt% HMTHP in water as feed), which is denoted as *operando* conditions.

For the Rh/C catalyst, XANES and EXAFS spectra were collected in He after pretreatment in flowing H_2 at various temperatures in the range of 298 to 723 K. Rh is highly reduced (~50%) after pretreatment at 298 K, and Rh is fully reduced after pretreatment at 363 K. A Rh-Rh contribution at a bond distance of 2.67-2.68 Å is observed, similar to Rh foil. For the Re/C catalyst, the XANES and EXAFS spectra collected in He after pretreatment in flowing H_2 indicate that Re is fully oxidized after pretreatments in H_2 at 298 through 523 K. No Re-O contribution remained after reduction at 723 K, while a Re-Re contribution was detected with coordination number of 9.8 and bond distance of 2.74 Å, similar to the bond distance for Re foil. In general, these results indicate that monometallic Rh is highly reducible even at 298 K, while monometallic Re is highly oxophilic and does not easily reduce to the metallic state.

For the RhRe/C catalyst reduced at temperatures from 298 to 333 K, there is a Rh-O contribution with coordination number decreasing with increasing temperature from 3.2 to 0.4 indicative of partially oxidized Rh. Rh is reduced to the metallic state after pretreatment at temperatures higher than 333 K, in agreement with the XANES and similar to the temperature required to fully reduce monometallic Rh/C. The magnitude of the Fourier transforms (FTs) of the Rh EXAFS spectra for the RhRe/C catalyst pretreated at 393 to 723 K are shown in Figure 3a. The Rh portion of the catalyst is reduced with no evidence of Rh-O bonds. The fits of the spectra indicate the presence of a Rh-Re contribution in addition to Rh-Rh. The Rh-Rh coordination (ca. 5-6) is larger than that of Rh-Re (ca. 2-3), suggesting a Rh-core/Re-shell structure.

The magnitude of the FTs of the Re EXAFS spectra are shown in Figure 3b-c, and the fit of the EXAFS shows a Re-O contribution for the RhRe/C catalyst that decreases from 1.3 to 0.4 with increasing pretreatment temperature (298 -333 K). The Re-O bond distance (1.74 Å) is consistent with a Re(VII) oxide double bond, i.e., Re=O. The Re-O contribution and its corresponding low coordination number suggest that a mixture of Re states are present. The Re-O contribution is not apparent after pretreatment temperatures above 363 K, suggesting that Re is reduced at relatively low temperatures (< 393 K), in agreement with the XANES edge energies and linear component analysis. The conclusion that Re is highly reduced was also in agreement with delta-XANES and delta-EXAFS analyses. The ease of Re reduction in RhRe/C compared to monometallic Re/C suggests that all Re is in contact with metallic Rh in RhRe/C in accordance with EDS results.[1] The Re-Re coordination number increased from 1.3 to 4.3 with increasing pretreatment temperature (298 - 723 K), and had a bond distance of 2.57 Å which is significantly contracted compared to that for Re foil (2.75 Å). In addition, a Re-Rh contribution was observed with coordination number of 2.4-3.9, increasing with temperature (298 -723 K), with a bond distance of 2.63 Å, which is equal to the sum of the atomic radii of Rh-Rh and Re-Re distances. The direct bonding between Rh and Re after reduction has been previously suggested for similar reduced catalysts (e.g., $RhRe/SiO_2$).[6]

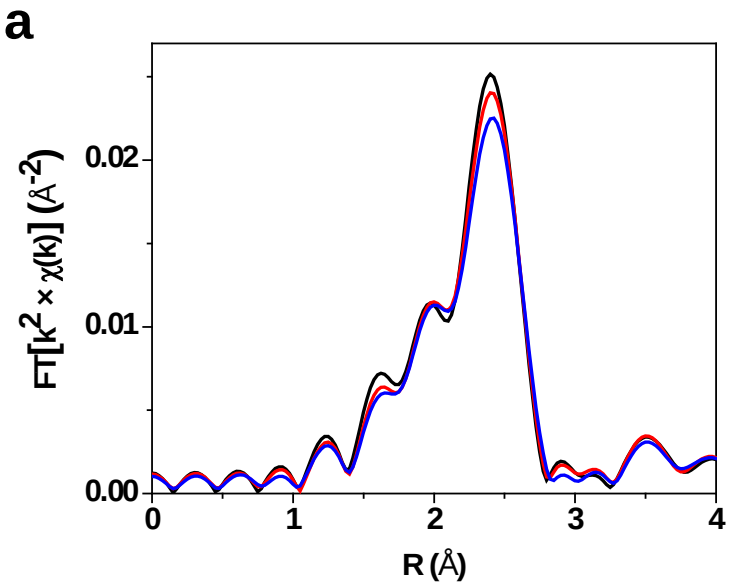
a
0.02
0.01
0.00
FT[k2 × χ(k)] (Å-2)
0
1
2
3
4
R (Å)

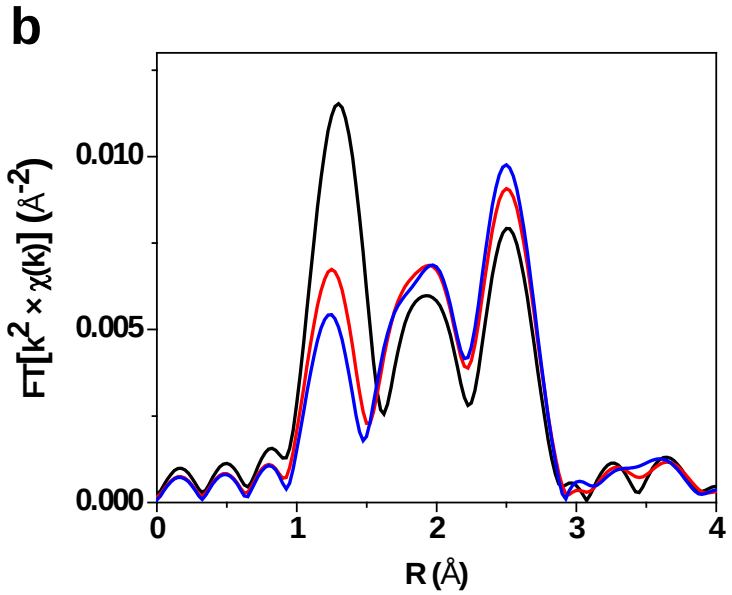
b
0.010
0.005
0.000
FT[k2 × χ(k)] (Å-2)
0
1
2
3
4
R (Å)

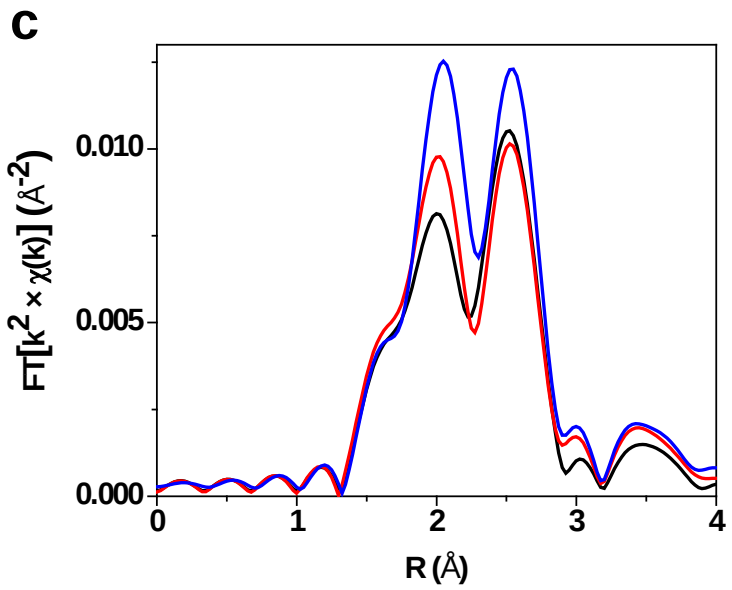

Figure 3| Magnitude of k^2-weighted FT of EXAFS data of (a) Rh K-edge of RhRe/C catalyst reduced at 393 K (black), 523 K (red), and 723 K (blue) (Δk = 2.5 – 13.8 Å^{-1}). Re L_{III} edge of RhRe/C catalyst reduced at (b) 298 K (black), 313 K (red), and 333 K (blue) (Δk = 2.8 – 11.9 Å^{-1}), and (c) 393 K (black), 523 K (red), and 723 K (blue) (Δk = 2.7 – 13.3 Å^{-1}).

From this work, we propose a model that is consistent with the XAS data and explains the reactivity trends observed with increasing reduction temperature. Specifically, the combination of EXAFS data and the observation that catalytic activity decreases with increasing reduction temperature suggests that Re is located preferentially at the surface for low reduction temperatures, and the surface concentration of Re then decreases with increasing reduction temperature. This behavior is reversible upon re-oxidation of the catalyst, because of the strong affinity of Re for oxygen. From the EXAFS data, at lower reduction temperatures, the coordination of Re-Re is lower than the coordination of Rh-Rh and Re-Rh, consistent with a Rh-rich core and a Re-rich shell structure. As pretreatment temperatures increase above 363 K, Re-Re coordination increases as Rh-Rh coordination decreases, indicating that Re penetrates into the center of the particle from the surface. This behavior is further supported by the fact that the total coordination number for Re increases as temperature increases.

We also collected XAS measurements of this catalyst under *operando* conditions for hydrogenolysis of HMTHP in liquid water at 393 K using RhRe/C catalyst pretreated at 523 and 723 K. The EXAFS fits of these data were indistinguishable from the *in situ* results; however, the data from these *operando* experiments could only be collected over a more narrow *k*-range, making it difficult to detect small contributions from Re-OH scattering. However, from the *operando* measurements, the XANES edge energies provided strong evidence for a fully reduced catalyst without any surface hydroxyls. Figure 4a and 4b show the XANES of the RhRe/C catalyst reduced at 523 K under *in situ* and *operando* conditions at both the Rh and Re edges. The spectra indicate that Rh and Re are fully reduced. Accordingly, it appears that Re does not form Re-OH to a measurable extent under reaction conditions for catalytic hydrogenolysis.

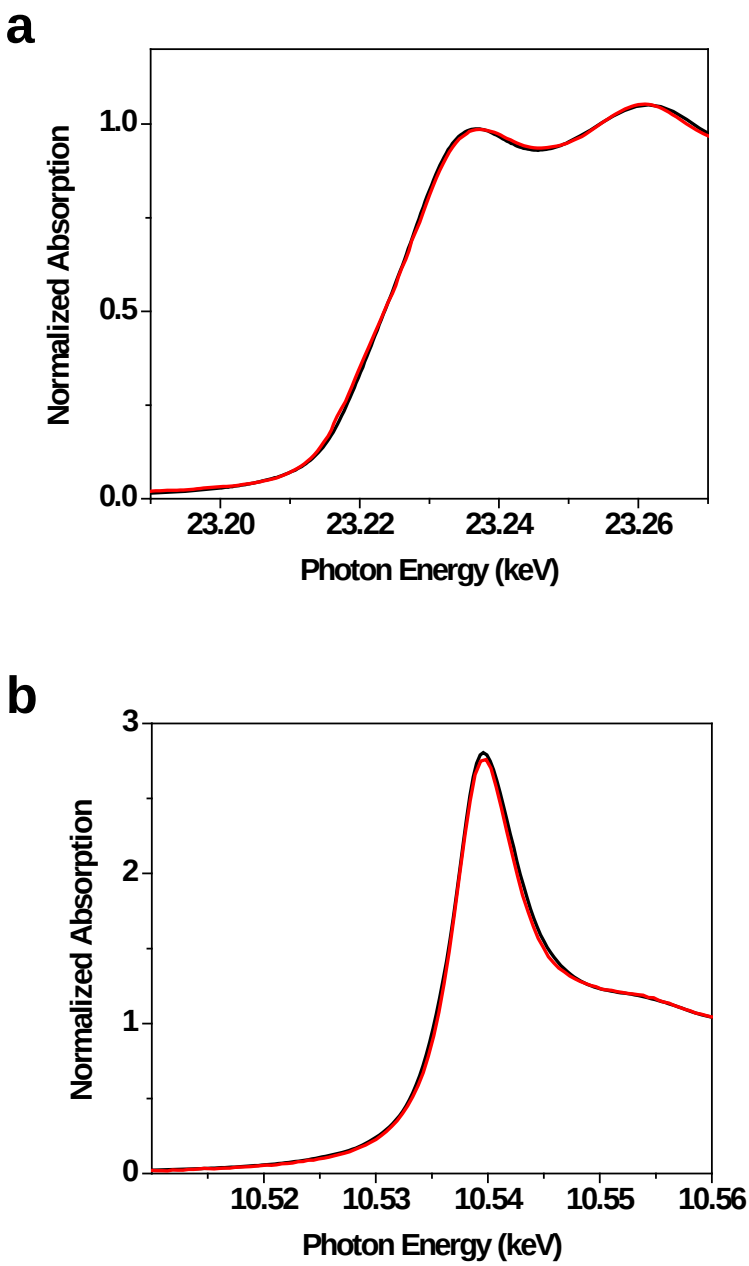

Figure 4| (a) Rh K-edge XANES (23.19 – 23.27 keV) of RhRe/C reduced at 523 K with spectra acquired under *in situ* conditions (black), and RhRe/C reduced at 523 K with spectra acquired under *operando* C-O hydrogenolysis conditions (red). (b) Re L_{III}-edge XANES (10.51 – 10.56 keV) of RhRe/C reduced at 523 K with spectra acquired under *in situ* conditions (black), and RhRe/C reduced at 523 K with spectra acquired under *operando* C-O hydrogenolysis conditions (red).

To further probe the apparent acidity of RhRe/C, we studied fructose dehydration to HMF,[2-5] a Brønsted acid-catalyzed probe reaction of relevance to biomass conversion. This study of fructose dehydration at 403 K was carried out over RhRe/C pretreated at 523 K in

flowing H_2 prior to initiation of liquid feed flow. A single-phase reaction solvent consisting of a mixture of tetrahydrofuran (THF) and water (mass ratio of THF: water = 4:1) was employed, because this solvent system was shown previously to be effective for fructose dehydration to HMF under continuous-flow conditions.[7] The RhRe/C catalyst displayed high activity for conversion of fructose to HMF, with selectivity to HMF maintained at approximately 50% at a conversion level of 30%, comparable to previous work with traditional acid catalysts.[7] Significantly, the RhRe/C catalyst was stable for at least 250 hours of time on stream. The formation of HMF from fructose provides further evidence of Brønsted acidity over RhRe/C.

The results from XAS measurements demonstrated that increasing pretreatment temperatures in H_2 was accompanied by an increase in the coordination numbers of the Rh-Re (313 - 723 K, 1.6-2.8) and Re-Rh (298 - 723 K, 2.4-3.9) contributions. Our reaction kinetics results demonstrate that these increases in Re coordination to Rh and total Re coordination as temperature increases correlate with a decrease in activity for C-O hydrogenolysis over RhRe/C. These changes are also accompanied by a decrease in site density as measured by NH_3 TPD. Therefore, the results from reaction kinetics and XAS indicate that the presence of low coordination Re on the surface of Rh particles is responsible for the high catalytic activity of RhRe/C for C-O hydrogenolysis and dehydration reactions. As reduction temperature increases, Re coordination increases indicating its migration into the nanoparticle which results in a decrease in catalytic activity.

An important result of our studies is that the XAS results for RhRe/C show no evidence of Re-O coordination after pretreatment at 363 K and above, even under *operando* conditions. Therefore, oxidized rhenium does not appear to be necessary to impart acidic functionality to the catalyst. In view of the oxophilic nature of Re compared to Rh, we suggest that the apparent acidity of RhRe/C may be generated by the activation of water molecules through interaction of the O atom in water with small clusters or even single atoms of Re on the surface of metallic Rh (i.e., Re-Rh species). The activation of water over Re in similar catalysts (e.g., $PtRe/TiO_2$) has been previously reported.[8] An increase in the pretreatment temperature from 393 K to 723 K leads to an increase in Re coordination from 6.0 to 8.2 and therefore a decrease in activity due to a loss of low coordination Re sites on the surface of Rh that we believe are capable of water activation.

To investigate the influence of water on catalytic activity, we performed reaction kinetics experiments for C-O hydrogenolysis of HMTHP over RhRe/C using solvents consisting of THF/water mixtures of varying composition. As shown in Figure 5, C-O hydrogenolysis activity over RhRe/C steadily decreases with decreasing water concentration. Importantly, no hydrogenolysis activity was observed when dry THF was the solvent. The decrease in C-O hydrogenolysis activity with decreasing water concentration and the inactivity of RhRe/C under dry conditions provides further evidence of the role of water in conferring an acidic functionality over this catalyst. It is important to note that water is not a reactant, and instead, liquid water is required for high hydrogenolysis activity.

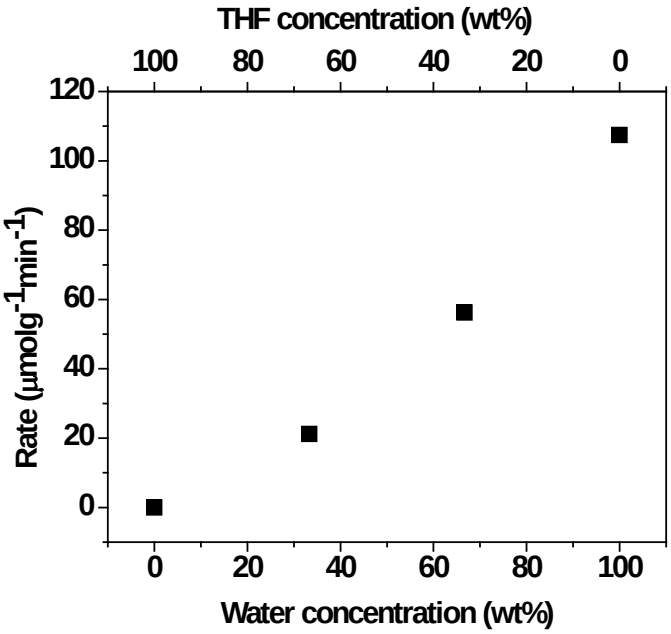

Figure 5| Rate of hydrogenolysis of HMTHP over RhRe/C with varying THF/water mixture compositions under batch reaction conditions. Catalyst pretreated under 34 bar H_2 at 393 K prior to introduction of liquid feed. Selectivities to 1,6-HDO were >90% for all data points. Reaction conditions: 5 wt% HMTHP in THF/water mixtures as feed, 393 K, 34 bar H_2.

2.2 Low temperature water-gas shift on platinum-rhenium alloys

Results from our group previously demonstrated that the low temperature water-gas shift over Pt takes place on a surface operating at high CO coverage, and water activation is a kinetically significant step. In light of previous insights regarding the addition of Re to form an alloy catalyst, we investigated the role of Re addition to Pt for this reaction (in collaboration with Manos Mavrikakis). This work used a combination of experiments, DFT calculations, and mean-field microkinetic modeling to elucidate the predominant surface reactions and species on platinum, with a focus on the elucidation of the factors that cause the increased activity of PtRe catalysts for this reaction.

Carbon supported PtRe catalysts were synthesized, and reaction kinetics were measured over a wide range of reaction conditions. As shown in Figure 6, we have been successful in capturing the behavior of all catalysts by adjusting only the most sensitive parameters for each system. We determined that the platinum catalyst operates at a CO coverage of ≈ 2/3 monolayers and is rate-limited by water activation, in agreement with the work of Grabow *et al*.[9]

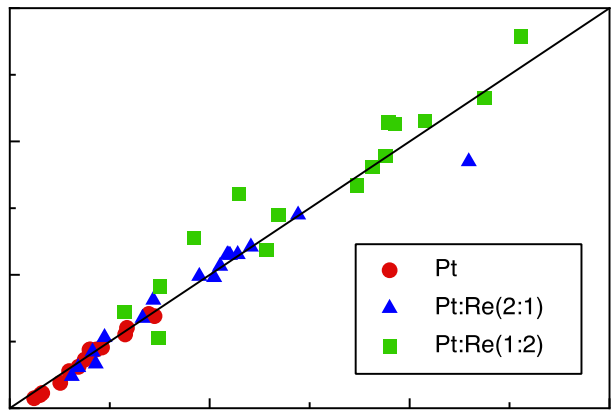

Figure 6| Calculated (model) versus experimental turnover frequency (TOF). The parameters used to calculate the model TOF are those obtained from fitting the experimental TOF's.

Interestingly, PtRe alloys show almost identical mechanistic behavior (the rate-limiting step is water activation), but the alloys display higher turn-over frequencies (TOF). During the modeling of the PtRe catalysts, we observed that the surface Re atoms are predicted to be highly covered under reaction conditions, and the promoting effect from rhenium is caused by destabilization of CO binding on adjacent platinum atoms.

Based on the results obtained from our microkinetic model we have constructed a reaction network for water-gas shift on the PtRe catalyst (Figure 7). All surface species and possible reactions included in our model are shown with the main pathway highlighted by solid arrows. One important aspect is that although lower energy pathways exist in the network, they are all limited by low OH coverage which is a consequence of water activation being the rate-limiting step.

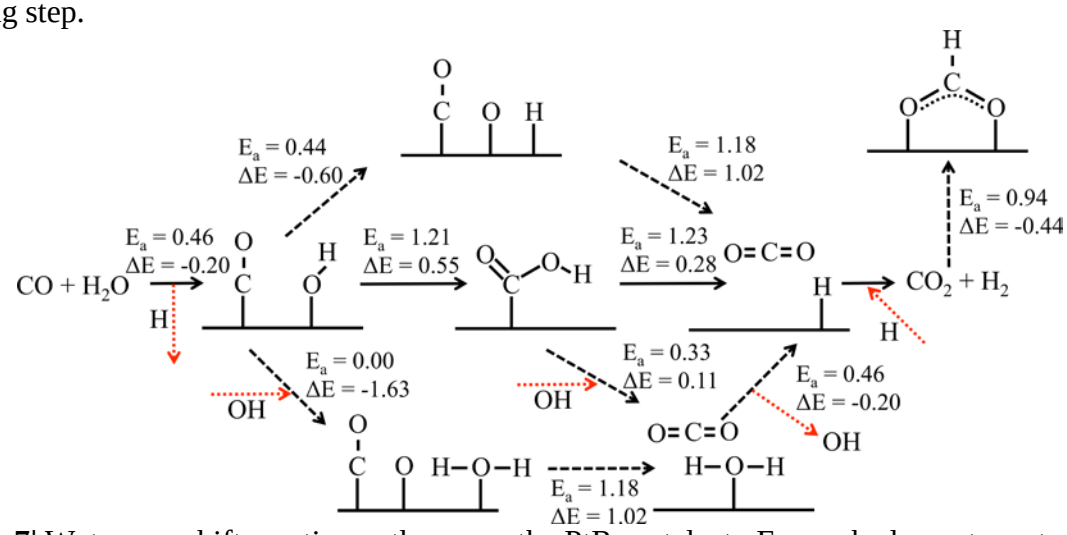

Figure 7| Water-gas shift reaction pathway on the PtRe catalyst. For each elementary step, activation energy barrier, Ea, and reaction energy, ΔE, are shown in eV based on the calculated DFT values. The COOH mediated pathway, highlighted by solid arrows, is found to be prevalent through a flux analysis from all microkinetic models. Species added or removed during an elementary step are shown with dotted red arrows. OH mediated pathways are

hindered by low OH coverage. Formate is a spectator species only produced after the main reaction products (CO_2 and H_2) have been formed.

2.3 Stabilization of copper catalysts by Atomic Layer Deposition (ALD)

ALD is a self-limiting growth process that creates highly conformal coatings.[10] In our recent work, ALD overcoats were deposited (in collaboration with Jeff Elam at Argonne National Laboratory and Tom Kuech at the University of Wisconsin) onto oxidized copper nanoparticles supported on γ-Al_2O_3. The catalyst was reduced in flowing H_2 and passivated in dilute O_2 (Figure 8a) before the overcoat was deposited using 45 alternating cycles of trimethylaluminum (TMA) and water, leaving the metal nanoparticles completely encapsulated in an amorphous alumina overcoat (Figure 8b). Treatment (in oxygen or inert gas) at 973 K produced porosity in the overcoat, thereby providing access to the underlying copper particles (Figure 8c). Evidence of this porosity is provided (in collaboration with Paul Voyles at the University of Wisconsin) by STEM and STEM/EELS, where the porosity of an alumina overcoat produced by ALD on Cu/SiO_2 is probed by subsequent deposition of niobia by ALD. The penetration depth into the alumina overcoat of niobia deposited on an overcoated and calcined sample (Figure 8e, 2.0 ± 1.0 nm), as measured by STEM/EELS, is greater than the penetration depth of niobia deposited on an uncalcined sample (Figure 8e, 1.0 ± 0.8 nm), indicating the formation of porosity upon calcination.

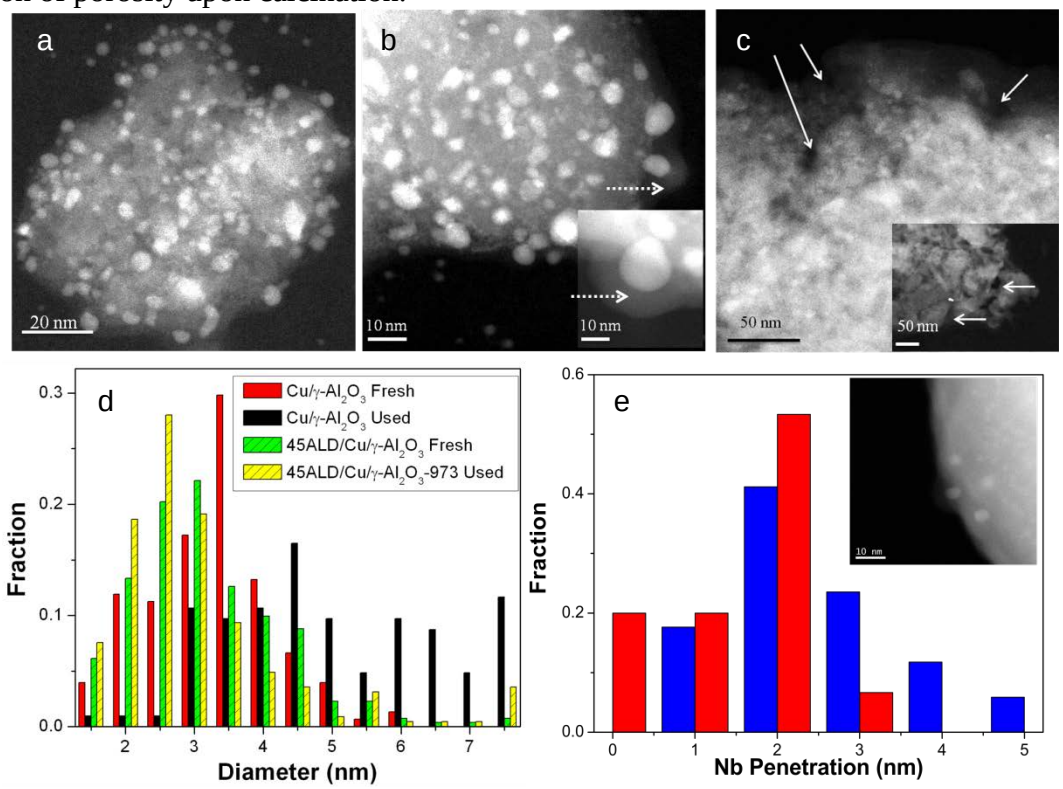

Figure 8| STEM images (a) Cu/γ-Al_2O_3, (b) 45ALD/Cu/γ-Al_2O_3, (c) 45ALD/Cu/γ-Al_2O_3-973, and (d) the particle size distributions of fresh and used catalysts. Dashed arrows point to the ALD overcoat, and solid arrows indicate pores in the overcoat. (e) Penetration depth of 20 ALD cycles of niobia deposited on 30ALD/Cu/SiO_2 (red) and 30ALD/Cu/SiO_2-973 (blue), as measured by STEM/EELS. The inset is a STEM image of 30ALD/Cu/SiO_2.

Prior to ALD overcoating, the total surface area of copper supported on γ-Al_2O_3 (Cu/γ-Al_2O_3, 5 wt%) was 190 m^2 g^{-1}, and the total pore volume was 0.45 cm^3 g^{-1}. After reduction in H_2 at 573 K, Cu/γ-Al_2O_3 had 86 μmol g^{-1} of surface Cu^0 sites, as titrated by N_2O flow chemisorption.[11] For ALD overcoated samples (45ALD/Cu/γ-Al_2O_3, 2.5 wt%), surface area and pore volume decreased (16 m^2 g^{-1}, 0.03 cm^3 g^{-1}), indicating that the ALD process filled the pores of the support and created a continuous overcoat. Additionally, Cu^0 sites were not detected by N_2O titration after reduction in H_2 at 573 K. In contrast, following treatment at 973 K (45ALD/Cu/γ-Al_2O_3-973) in air, the surface area and pore volume increased (39 m^2 g^{-1}, 0.08 cm^3 g^{-1}), suggesting pore formation in the overcoat. Importantly, treatment at 973 K followed by H_2 reduction, re-exposed Cu^0 surface sites (23 μmol g^{-1}). The chemisorption and surface area measurements corroborate observations of the overcoat (Figure 8b) and pore formation (Figure 8c) from STEM and STEM/EELS.

The catalytic properties of Cu/γ-Al_2O_3 and 45ALD/Cu/γ-Al_2O_3-973 were studied for the liquid phase hydrogenation of furfural to furfuryl alcohol in 1-butanol as the solvent (403 K, 22 bar H_2). This reaction was chosen as an example of an industrially-relevant copper-catalyzed hydrogenation that would benefit from stabilized copper catalysts.[12] Figure 9a shows that Cu/γ-Al_2O_3 deactivated during reaction in a continuous-flow reactor. Deactivation by the deposition of carbonaceous species (i.e., coke) on the catalyst is reversible upon calcination, whereas deactivation by leaching or sintering of copper is irreversible. The deactivation of Cu/γ-Al_2O_3 displayed in Figure 9a (open symbols) is not completely reversible upon calcination followed by reduction in H_2, suggesting that sintering and leaching have occurred.

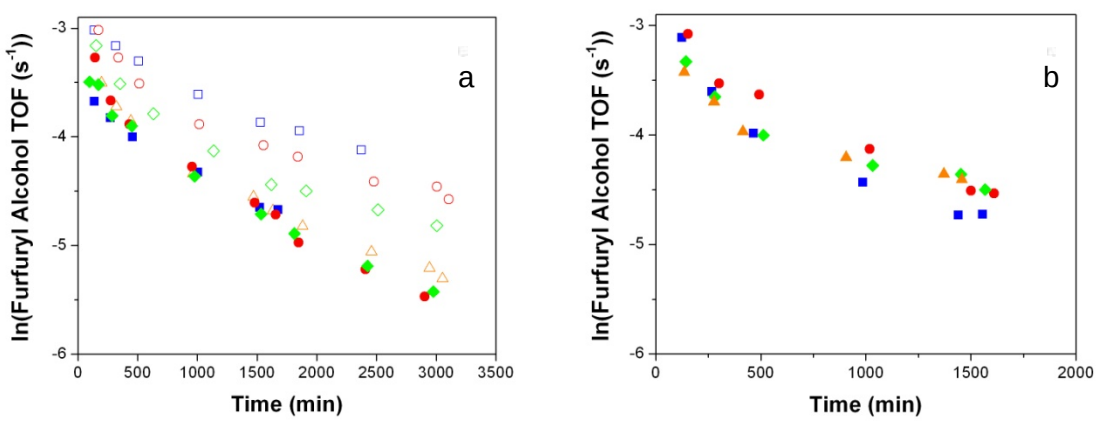

Figure 9| (a) Furfural hydrogenation in liquid butanol at 403 K and 22 bar H_2 using Cu/γ-Al_2O_3 (fresh □, regenerated x 1 ○, regenerated x 2 ◊, regenerated x 3 △) and 45ALD/Cu/γ-Al_2O_3-973 (fresh ■, regenerated x 1 ●, regenerated x 2 ♦). (b) Furfural hydrogenation in liquid water using 45ALD/Cu/γ-Al_2O_3-973 (fresh ■, regenerated x 1 ●, regenerated x 2 ♦, regenerated x 3 ▲) at the same reaction conditions. TOF is calculated using initial sites of a fresh, unused catalyst.

STEM was used to measure the particle size distribution of the copper nanoparticles before and after reaction and confirmed sintering. As seen in Figure 8d, the size of the Cu/γ-Al_2O_3 particles was 3 ± 1 nm before reaction and increased to 5 ± 2 nm after three cycles of reaction and regeneration. The metal loading of the catalysts was analyzed by inductively-coupled plasma atomic emission spectroscopy (ICP-AES). The copper loading of Cu/γ-Al_2O_3 was 5.9 ± 0.2% before reaction and 5.0 ± 0.2% after 3 cycles of reaction and regeneration, indicating leaching of copper from the catalyst.

The stability of 45ALD/Cu/γ-Al_2O_3-973 differs substantially from Cu/γ-Al_2O_3 under the same reaction and regeneration conditions. The initial activity of 45ALD/Cu/γ-Al_2O_3-973 was fully recovered after calcination and re-reduction (Figure 9a, filled symbols). The copper particle size was 3 ± 1 nm before and after three cycles of reaction with intermediate regeneration (Figure 8d), confirming that the overcoat prevented sintering. Furthermore, the copper loading of the catalyst measured by ICP-AES was 2.4 ± 0.1% before reaction and 2.5 ± 0.1% after reaction, indicating that the overcoat eliminated copper leaching. (The loading of 45ALD/Cu/γ-Al_2O_3-973 is lower due to the mass of alumina added by ALD.) Also, in a control experiment, the Cu/γ-Al_2O_3 catalyst without an ALD overcoat exhibited irreversible deactivation after calcination pretreatment at 973 K, demonstrating that the overcoat, not the high temperature calcination treatment, is responsible for stabilization of 45ALD/Cu/γ-Al_2O_3-973. The ALD overcoat also stabilizes the copper nanoparticles against sintering and leaching in the more demanding environment of high temperature liquid water (Figure 9b).

Solid state ^{27}Al magic angle spinning nuclear magnetic resonance (MAS-NMR) spectroscopy and XRD were employed (in collaboration with Susannah Scott at the University of California-Santa Barbara) to probe the mechanism that leads to pore formation. Alumina was deposited on copper supported on TiO_2 (45ALD/Cu/TiO_2, Figure 10a) to eliminate signals from the support and to demonstrate the restructuring of the overcoat (45ALD/Cu/γ-Al_2O_3 is qualitatively the same, discussion omitted for brevity). Figure 10a shows that 6-, 5-, and 4-coordinate aluminum atoms are present in the overcoat (resonances at 9.3, 33.3, and 65.5 ppm, respectively). The presence of 5-coordinate aluminum before calcination is consistent with an amorphous overcoat.[13] After calcination at 973 K, the resonance corresponding to 5-coordinate aluminum disappears and the ratio of 6- to 4- coordinate aluminum suggests crystallization.[14] Results from XRD (Figure 10b) show that the overcoat undergoes crystallization during heating at 973 K, as evidenced by reflections due to γ-Al_2O_3. The crystallization creates voids in the overcoat as it becomes more dense, exposing the underlying copper.[15]

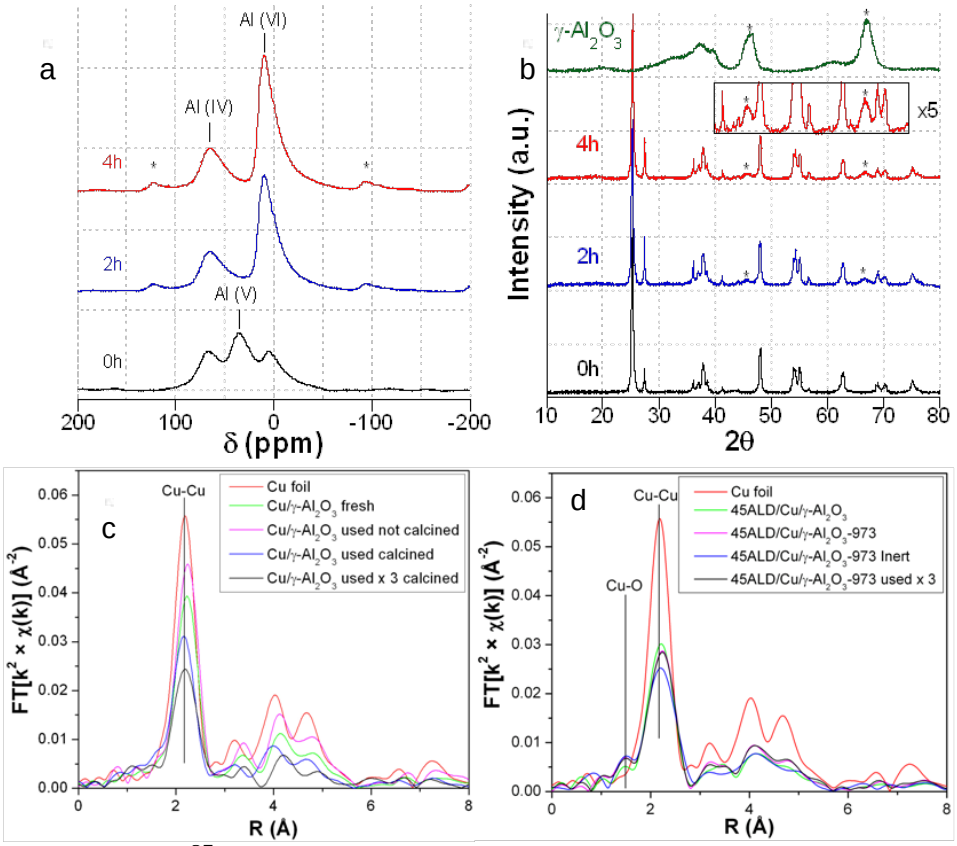

Figure 10| Solid-state ^{27}Al MAS-NMR spectra of (a) 45ALD/Cu/TiO_2 prior to (black) and after calcination at 973K (2 h, blue; 4 h, red). Spinning sidebands are indicated by *. (b) Powder X-ray diffraction patterns for γ-Al_2O_3 (green) and 45ALD/Cu/TiO_2 prior to (0 h, black) and after calcination (2h, blue; 4h, red). A magnified spectrum for 45ALD/Cu/TiO_2 (5×) is also presented, highlighting the γ-Al_2O_3. The k^2-weigthed EXAFS in *R*-space of (c) Cu/γ-Al_2O_3 and (d) overcoated catalysts after different stages of synthesis and use. Cu foil EXAFS is shown for comparison.

Sintering and leaching of metal nanoparticles are believed to originate from under-coordinated copper surface atoms located at edges, corners, and defects.[16] Accordingly, stability imparted to the copper nanoparticles by ALD overcoating may result from selective interactions of the overcoat with under-coordinated copper atoms that remain after pore opening.[17, 18] The interaction of the alumina overcoat with the copper nanoparticle was probed (in collaboration with Fabio Ribeiro at Purdue University and Jeff Miller at Argonne National Laboratory) using X-ray absorption near edge spectroscopy (XANES) and X-ray absorption fine structure spectroscopy (EXAFS). According to XANES and EXAFS curve fits, Cu/γ-Al_2O_3 was fully reduced by pretreatment in H_2 at 573 K (Figure 10c, green). The same behavior was observed for 45ALD/Cu/γ-Al_2O_3 (Figure 10d, green). Thus, the overcoating was sufficiently porous for H_2 diffusion; however, larger molecules cannot penetrate the overcoat (i.e., low surface area and no titration of Cu(0)). Calcination at 973 K led to the formation of a copper oxide species that was not reduced by treatment in H_2 at 573 K (Figure 10d). The presence of Cu-O scattering after treatment at 973 K and reduction in H_2 indicates that the high temperature treatment led to strong interactions between the alumina overcoat and the copper nanoparticles. Moreover, stable

copper-oxygen bonds also formed during treatment at high temperature in inert atmosphere (45ALD/Cu/γ-Al_2O_3-973Inert, Figure 10d, blue), indicating that the oxygen is from alumina.

After reduction but prior to reaction, the EXAFS spectra for Cu/γ-Al_2O_3 and 45ALD/Cu/γ-Al_2O_3 (Figure 10c and Figure 10d, green) are similar. During reaction, the copper nanoparticles on Cu/γ-Al_2O_3 (Figure 10c, magenta) had sintered, as demonstrated by an increase in Cu-Cu coordination. Following catalyst regeneration by calcination and reduction, (Figure 10c, blue and black) the Cu-Cu coordination decreased due to re-dispersion of the oxidized copper and the loss of copper due to leaching during reaction. In contrast, the used 45ALD/Cu/γ-Al_2O_3-973 catalyst (Figure 10d, black) appears unchanged after reaction.

Scanning tunneling microscopy (STM) on a Cu(111) surface was used (in collaboration with Peter Stair at Northwestern University and Jeff Elam at Argonne National Laboratory) to probe the interactions of alumina with the surface and to observe the nanoscale changes of the ALD alumina after high temperature treatment. Alumina clusters were observed after four alternating exposures of water and TMA on the surface of a Cu(111) surface that had been pre-oxidized and hydrated (Figure 11a). The height profile line scans in Figure 11c and Figure 11d, (corresponding to blue lines in Figure 11a and Figure 11b) indicate that alumina preferentially decorated the step edges and defects of the Cu(111) surface. After four cycles, alumina occupied 59 ± 3% of terrace sites and 91± 1% of edge and defect sites. When this surface was heated to 773 K under ultra-high vacuum, the coverage of Cu(111) terraces decreased relative to edges (30 ± 4% of terraces vs. 80± 3% of edges and defects, Figure 11b). These results support the conclusion that alumina preferentially armors under-coordinated copper (e.g. steps), leaving terraces mostly open after annealing.

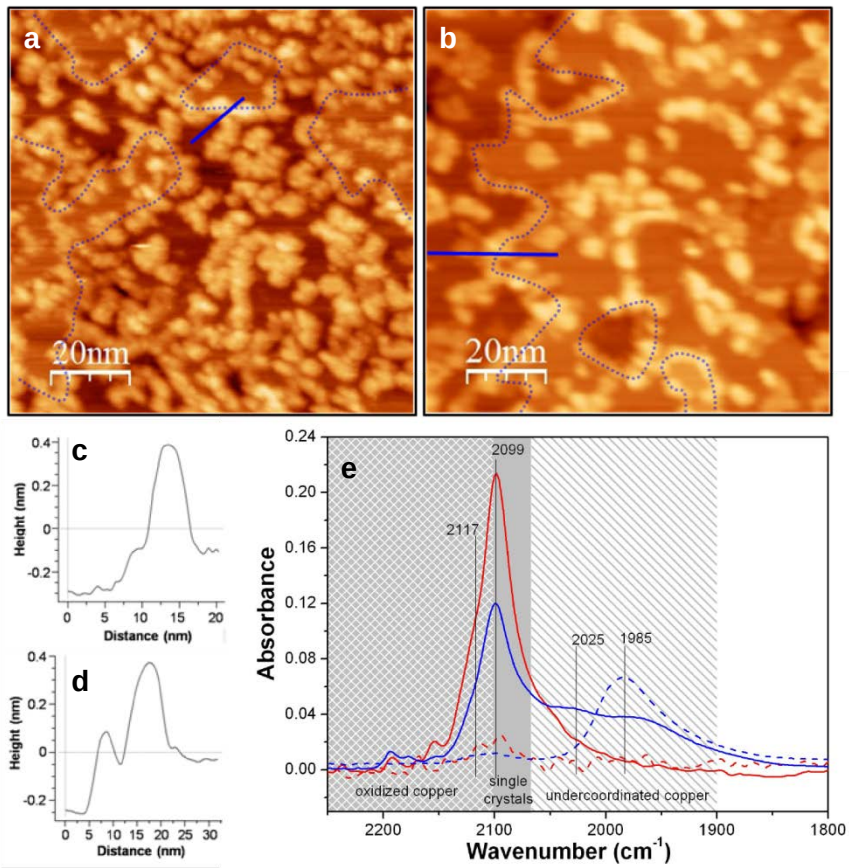

Figure 11| (a) STM image of an oxidized and hydrated Cu(111) surface after exposure to four cycles of TMA and water. (b) STM image after annealing at 773 K in vacuum. The dashed lines in the images highlight the step edges; (c and d) the height profiles along the solid blue lines (for a and b, respectively) indicate the position of a step edge. (e) IR bands for CO adsorbed on Cu/γ-Al_2O_3 (blue) and 45ALD/Cu/γ-Al_2O_3-973 (red) at 123 K (solid) and 283 K (dashed). The intensities are normalized by the pellet density and copper loading. Shaded regions indicate typical wavenumbers for CO adsorbed at different types of copper surface sites.

The surface of the copper nanoparticles was further probed using FTIR spectroscopy of adsorbed CO. The main features of the IR spectra of CO adsorbed on Cu/γ-Al_2O_3 at 123 K were a band at 2099 cm^{-1} with a shoulder at 2117 cm^{-1} and a broad absorption at lower wavenumber (Figure 11e, blue). The band at 2099 cm^{-1} is typical of CO adsorbed on oxide-supported copper particles. In single crystal studies, Hollins *et al.* demonstrated that these bands arise from high coverage of CO adsorbed on sites of a Cu(111) surface near oxygen (2117 cm^{-1}) and far from oxygen (2099 cm^{-1}).[19] In agreement with these assignments, Kim *et al.* assigned bands at 2091 and 2116 cm^{-1} to CO adsorbed on a Cu(100) surface decorated with oxygen.[20] DFT calculations (in collaboration with Manos Mavrikakis at the University of Wisconsin and Jeff Greeley at Purdue University) for the stretching frequencies of CO adsorbed on various copper sites near AlO_x moieties confirmed that the CO band shifts to higher wavenumbers when the CO is located closer to AlO_x on the surface (Figure 12). Consequently, the band at 2099 cm^{-1} and the shoulder at 2117 cm^{-1} for Cu/γ-Al_2O_3 are assigned to adsorption of CO on copper terrace sites and copper near the support. The broad absorption at lower wavenumbers is assigned to CO adsorbed on highly under-coordinated copper sites on the catalyst surface.[21-23] The band at 2099 cm^{-1} disappeared as the sample was warmed to 283 K, confirming its assignment to Cu^0 and not Cu^+. The broad band at lower wavenumber remained upon warming due to the strong binding of CO to highly under-coordinated copper sites.

The FTIR spectrum for CO adsorbed on 45ALD/Cu/γ-Al_2O_3-973 at 123 K is dominated by the band at 2099 cm^{-1}. Importantly, the relative intensity of the band at 2099 cm^{-1} compared to the broad absorption at lower wavenumber indicates that the highly under-coordinated copper sites responsible for sintering and leaching were selectively covered by the ALD overcoating procedure.

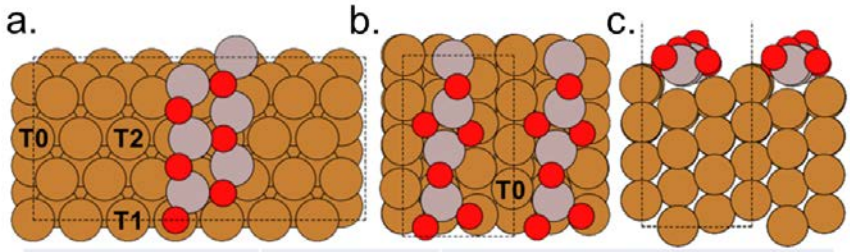

Surface	Site	CO stretching frequency (cm^{-1})
AlO/Cu(111)	T0	2016
AlO/Cu(111)	T1	2031
AlO/Cu(111)	T2	2024
Cu(111)	Top	2007
Al_2O_3/Cu(211)	T0	2085
Cu(211)	Step Top	2018
CO gas	CO gas	2156

Figure 12| (a) Top view of AlO_x/Cu(111) (b) Top view and (c) side view of AlO_x/Cu(211). CO vibrational frequencies calculated from DFT (VASP) at atop sites on the various model surfaces are reported in the table. For comparison, the stretching frequencies of CO in the gas phase and CO on Cu(111) and Cu(211) are included. Black dotted lines indicate periodic unit cells used in calculations. Gray, red and copper spheres represent Al, O and Cu, respectively.

References

1. M. Chia, Y. J. Pagan-Torres, D. Hibbitts, Q. Tan, H. N. Pham, A. K. Datye, M. Neurock, R. J. Davis and J. A. Dumesic, *Journal of the American Chemical Society*, 2011, **133**, 12675-12689.
2. B. F. M. Kuster and H. M. G. Temmink, *Carbohydrate Research*, 1977, **54**, 185-191.
3. B. F. M. Kuster and H. S. van der Baan, *Carbohydrate Research*, 1977, **54**, 165-176.
4. Y. Román-Leshkov, J. N. Chheda and J. A. Dumesic, *Science*, 2006, **312**, 1933-1937.
5. J. N. Chheda, Y. Roman-Leshkov and J. A. Dumesic, *Green Chemistry*, 2007, **9**, 342-350.
6. S. Koso, H. Watanabe, K. Okumura, Y. Nakagawa and K. Tomishige, *The Journal of Physical Chemistry C*, 2011, **116**, 3079-3090.
7. M. H. Tucker, A. J. Crisci, B. N. Wigington, N. Phadke, R. Alamillo, J. Zhang, S. L. Scott and J. A. Dumesic, *ACS Catalysis*, 2012, **2**, 1865-1876.
8. K. G. Azzam, I. V. Babich, K. Seshan, B. L. Mojet and L. Lefferts, *ChemCatChem*, 2013, **5**, 557-564.
9. L. C. Grabow, A. A. Gokhale, S. T. Evans, J. A. Dumesic and M. Mavrikakis, *Journal of Physical Chemistry C*, 2008, **112**, 4608-4617.
10. R. L. Puurunen, *J. Appl. Phys.*, 2005, **97**, 121301-121352.
11. G. C. Chinchen, C. M. Hay, H. D. Vandervell and K. C. Waugh, *J. Catal.*, 1987, **103**, 79-86.
12. K. J. Zeitsch, *The chemistry and technology of furfural and its many by-products*, Elsevier, Amsterdam, Netherlands, 2000.
13. E. W. Hagaman, J. Jiao, B. Chen, Z. Ma, H. Yin and S. Dai, *Solid State Nucl. Mag.*, 2010, **37**, 82-90.
14. C. Pecharroman, I. Sobrados, J. E. Iglesias, T. Gonzalez-Carreno and J. Sanz, *J. Phys. Chem. B*, 1999, **103**, 6160-6170.
15. L. B. Skinner, A. C. Barnes, P. S. Salmon, L. Hennet, H. E. Fischer, C. J. Benmore, S. Kohara, J. K. R. Weber, A. Bytchkov, M. C. Wilding, J. B. Parise, T. O. Farmer, I. Pozdnyakova, S. K. Tumber and K. Ohara, *Phys. Rev. B*, 2013, **87**, 024201.
16. J. Greeley, *Electrochim. Acta*, 2010, **55**, 5545-5550.
17. J. Lu, B. Fu, M. C. Kung, G. Xiao, J. W. Elam, H. H. Kung and P. C. Stair, *Science*, 2012, **335**, 1205-1208.
18. J. Lu, B. Liu, J. P. Greeley, Z. Feng, J. A. Libera, Y. Lei, M. J. Bedzyk, P. C. Stair and J. W. Elam, *Chem. Mater.*, 2012, **24**, 2047-2055.
19. P. Hollins and J. Pritchard, *Surf. Sci.*, 1983, **134**, 91-108.
20. C. M. Kim, C. W. Yi and D. W. Goodman, *J. Phys. Chem. B*, 2005, **109**, 1891-1895.
21. F. Boccuzzi, G. Ghiotti and A. Chiorino, *Surf. Sci.*, 1985, **156, Part 2**, 933-942.
22. G. Ghiotti, F. Boccuzzi and A. Chiorino, *Stud. Surf. Sci. Catal.*, 1985, **Volume 21**, 235-246.
23. K. Hadjiivanov, T. Venkov and H. Knözinger, *Catal. Lett.*, 2001, **75**, 55-59.

24. J. S. Luterbacher, J. M. Rand, D. Martin Alonso, J. Han, J. T. Youngquist, C. T. Maravelias, B. F. Pfleger, and J. A. Dumesic, *Science*, 2014, **343**, 277-280.
25. J. Wang, V. F. Kispersky, W. Nicholas Delgass and F. H. Ribeiro, *J. Catal.*, 2012, **289**, 171-178.
26. M. Shekhar, J. Wang, W. S. Lee, W. D. Williams, S. M. Kim, E. A. Stach, J. T. Miller, W. N. Delgass and F. H. Ribeiro, *Journal of the American Chemical Society*, 2012, **134**, 4700-4708.
27. S. Singh, S. Li, R. Carrasquillo-Flores, A. C. Alba-Rubio, J. A. Dumesic, and M. Mavrikakis, *AIChE Journal*, 2014, **60,** 1303-1319.
28. W. D. Williams, L. Bollmann, J. T. Miller, W. N. Delgass, F. H. Ribeiro, *Applied Catalysis B: Environmental*, 2012, **125**, 206– 214.
29. A. J. Medford, A. C. Lausche, F. Abild-Pedersen, B. Temel, N. C. Schjødt, J. K. Nørskov, F. Studt, *Topics in Catalysis*, 2014, **57**, 135–142.
30. J. Su, W. Mao, X.-C. Xu, Z. Yang, H. Li, J. Xu, and Y.-F. Han, *AIChE Journal*, 2014, **60**, 1797-1809.
31. J. Wang, P. A. Chernavskii, A. Y. Khodakov, Y. Wang, *Journal of Catalysis* 2012, **286,** 51–61.
32. T. Shishido, T. Kitano, K. Teramura and T. Tanaka, *Catalysis Letters*, 2009, **129**, 383-386.
33. T. Shishido, T. Kitano, K. Teramura and T. Tanaka, *Topics in Catalysis*, 2010, **53**, 672-677.

Publications from DOE grant: 2011 - 2014
Total = 57

Joint funding with DOE:

Reaction Kinetics of Ethylene Glycol Reforming over Platinum in the Vapor versus Aqueous Phases, *Journal of Physical Chemistry C* **115**, 961 (2011), Shampa Kandoi, Jeff Greeley, Dante Simonetti, John Shabaker, Manos Mavrikakis, and J. A. Dumesic.

Activation of Amberlyst-70 for alkene oligomerization in hydrophobic media, *Topics in Catalysis* **54**, 447 (2011), Jesse Q. Bond, David Martin Alonso, Eric Wang, and J. A. Dumesic.

Synthesis of highly ordered hydrothermally stable mesoporous niobia catalysts by atomic layer deposition, *ACS Catalysis* **1**, 1234 (2011), Yomaira J. Pagán-Torres, Jean Marcel R. Gallo, Dong Wang, Hien N. Pham, Joseph A. Libera, Christopher L. Marshall, Jeffrey W. Elam, Abhaya K. Datye, and J. A. Dumesic.

A Microkinetic Analysis and Mechanism for the Water Gas Shift Reaction over Copper Catalysts, *Journal of Catalysis* **281**, 1 (2011), Rostam J. Madon, Drew Braden, Shampa Kandoi, Peter Nagel, Manos Mavrikakis, and J. A. Dumesic.

Reactive extraction of levulinate esters and conversion to γ-valerolactone for production of liquid fuels, *Chemistry and Sustainability* **4**, 357 (2011), Elif I. Gürbüz, David Martin Alonso, Jesse Q. Bond, and J. A. Dumesic.

Catalytic routes for the conversion of biomass into liquid hydrocarbon transportation fuels, *Energy and Environmental Science* **4**, 83 (2011), Juan Carlos Serrano-Ruiz, and J. A. Dumesic.

Inter-conversion between γ-valerolactone and pentenoic acid combined with decarboxylation to form butene over silica/alumina, *Journal of Catalysis* **281**, 290 (2011), Jesse Q. Bond, Dong Wang, David Martin Alonso, and J. A. Dumesic.

Production of liquid hydrocarbon fuels by catalytic conversion of biomass-derived levulinic acid, *Green Chemistry* **7**, 1755 (2011), Drew J. Braden, Carlos A. Henao, Jacob Heltzel, Christos C. Maravelias, and J. A. Dumesic.

Conversion of hemicellulose to furfural and levulinic acid using biphasic reactors with alkylphenol solvents, *Chemistry and Sustainability* **5**, 383 (2012), Elif I. Gürbüz, Stephanie G. Wettstein, and J. A. Dumesic.

Catalytic Conversion of Lignocellulosic Biomass to Fuels: Process Development and Technoeconomic Evaluation, *Chemical Engineering Science* **67**, 57 (2012), S. Murat Sen, Carlos A. Henao, Drew J. Braden, Christos T. Maravelias, and J. A. Dumesic.

Atomic Layer Deposition of Titanium Phosphate on Silica Nanoparticles, *Journal of Vacuum Science and Technology A* **30** (2012), Monika K. Wiedmann, David H. K. Jackson, Yomaira J. Pagan-Torres, T. F. Kuech, and J. A. Dumesic.

RuSn bimetallic catalysts for selective hydrogenation of levulinic acid to γ-valerolactone, *Applied Catalysis B: Environmental* **117**, 321 (2012), Stephanie G. Wettstein, Jesse Q. Bond, David Martin Alonso, Hien N. Pham, Abhaya K. Datye, and J. A. Dumesic.

Aqueous Phase Glycerol Reforming by PtMo Bimetallic Nano-particle Catalyst: Product Selectivity and Structural Characterization, *Topics in Catalysis* **55**, 53 (2012), Paul J. Dietrich, Rodrigo J. Lobo-Lapidus, Tianpin Wu, Aslihan Sumer, M. Cem Akatay, Bradley R. Fingland, Neng Guo, Christopher L. Marshall, Eric Stach, Julius Jellinek, W. Nicholas Delgass, Fabio H. Ribeiro, Jeffrey T. Miller, and J. A. Dumesic.

Catalytic conversion of biomass using solvents derived from lignin, *Green Chemistry* **14**, 1573 (2012), Pooya Azadi, Ronald Carrasquillo-Flores, Yomaira J. Pagán-Torres, Elif I. Gürbüz, Ramin Farnood, and J. A. Dumesic.

Experimental and Theoretical Studies of the Acid-Catalyzed Conversion of Furfuryl Alcohol to Levulinic Acid in Aqueous Solution, *Energy and Environmental Science* **5**, 6981 (2012), Gretchen M. González Maldonado, Rajeev S. Assary, Larry A. Curtiss, and J. A. Dumesic.

Reaction kinetics studies of the conversions of formic acid and butyl formate over carbon-supported palladium in the liquid phase, *Journal of Catalysis* **290**, 193 (2012), Brandon J. O'Neill, Elif I. Gürbüz, and J. A. Dumesic.

Acid-Catalyzed Conversion of Furfuryl Alcohol to Ethyl Levulinate in Liquid Ethanol, *Energy and Environmental Science* **5**, 8990 (2012), Gretchen M. González Maldonado, Rajeev S. Assary, Larry A. Curtiss, and J. A. Dumesic.

A roadmap for conversion of lignocellulosic biomass to chemicals and fuels, *Current Opinion in Chemical Engineering* **1**, 218 (2012), Stephanie G. Wettstein, David Martin Alonso, Elif I. Gurbuz, and J. A. Dumesic.

Production of levulinic acid and gamma-valerolactone (GVL) from cellulose using GVL as a solvent in biphasic systems, *Energy and Environmental Science* **5**, 8199 (2012), Stephanie G. Wettstein, David Martin Alonso, Yuxuan Chong, and J. A. Dumesic.

Bimetallic catalysts for upgrading of biomass to fuels and chemicals, *Chemical Society Reviews* **41**, 8075 (2012), David Martin Alonso, Stephanie G. Wettstein, and J. A. Dumesic.

Production of Butene Oligomers as Transportation Fuels using Butene for Esterification of Levulinic Acid from Lignocellulosic Biomass: Process Synthesis and Technoeconomic Evaluation, *Green Chemistry* **14**, 3289 (2012), S. Murat Sen, Elif I. Gurbuz, Stephanie G. Wettstein, David Martin Alonso, Christos T. Maravelias, and J. A. Dumesic.

A Sulfuric Acid Management Strategy for the Production of Liquid Hydrocarbon Fuels via Catalytic Conversion of Biomass-derived Levulinic Acid, *Energy and Environmental Science* **5**, 9690 (2012), S. Murat Sen, David Martin Alonso, Stephanie G. Wettstein, Elif I. Gurbuz, Carlos A. Henao, Christos T. Maravelias, and J. A. Dumesic.

Integrated Conversion of Hemicellulose and Cellulose from Lignocellulosic Biomass, *Energy and Environmental Science* **6**, 76, (2013), David M. Alonso, Stephanie G. Wettstein, Elif I. Gurbuz, Max A. Mellmer, and J. A. Dumesic.

Catalytic upgrading of the light fraction of a simulated bio-oil over CeZrOx catalyst, *Applied Catalysis B: Environmental* **142-143**, 368 (2013), Sikander H. Hakim, Brent H. Shanks, and J. A. Dumesic.

Conversion of hemicellulose to furfural using solid acid catalysts in γ-valerolactone, a biomass-derived solvent, *Angewandte Chemie International Edition* **52**, 1270, (2013), Elif I. Gürbüz, Jean Marcel R. Gallo, David Martin Alonso, Stephanie G. Wettstein, Wee Y. Lim, and J. A. Dumesic.

Selective production of aromatics from alkylfurans over solid acid catalysts, *Heterogeneous, Homogeneous, and Bio-Catalysis (ChemCatChem)* **5**, 2044 (2013), Dong Wang, Christian Mårup Osmundsen, Esben Taarning, and J. A. Dumesic.

Production and upgrading of 5-hydroxymethylfurfural using heterogeneous catalysts and biomass-derived solvents, *Green Chemistry* **15**, 85 (2013), Jean Marcel R. Gallo, David Martin Alonso, Max A. Mellmer, and J. A. Dumesic.

Direct conversion of cellulose to levulinic acid and gamma-valerolactone using solid acid catalysts, *Catalysis Science & Technology* **3**, 927 (2013), David Martin Alonso, Jean Marcel R. Gallo, Max A. Mellmer, Stephanie G. Wettstein, and J. A. Dumesic.

Gamma valerolactone, a sustainable platform molecule derived from lignocellulosic biomass, *Green Chemistry* **15**, 584 (2013), David Martin Alonso, Stephanie G. Wettstein, and J. A. Dumesic.

Deactivation mechanistic studies of copper chromite catalyst for selective hydrogenation of 2-furfuraldehyde, *Journal of Catalysis* **299**, 336 (2013), Dongxia Liu, Dmitry Zemlyanov, Tianpin Wu, Rodrigo J. Lobo-Lapidus, Jeffrey T. Miller, Christopher L. Marshall, and J. A. Dumesic.

Aqueous Phase Glycerol Reforming with Pt and PtMo Bimetallic Nanoparticle Catalysts: The Role of the Mo Promoter, *Topics in Catalysis* **56**, 1814 (2013), P.J. Dietrich, T. Wu, A. Sumer, J. Jellinek, W.N. Delgass, F.H. Ribeiro, J.T. Miller, and J. A. Dumesic.

Production of furfural from lignocellulosic biomass using Beta Zeolite and biomass-derived solvent, *Topics in Catalysis* **56**, 1775 (2013), Jean Marcel R. Gallo, David M. Alonso, Max A. Mellmer, Jher Hau Yeap, Hui Chin Wong, and J. A. Dumesic.

A highly selective route to linear alpha olefins from biomass-derived lactones and unsaturated acids, *Chemical Communications* **49**, 7040 (2013), Dong Wang, Sikander Hakim, David Martin Alonso, and J. A. Dumesic.

Aqueous-phase hydrodeoxygenation of sorbitol: A comparative study of Pt/Zr phosphate and Pt-ReOx/C, *Journal of Catalysis* **304**, 72 (2013), Yong Tae Kim, George W. Huber, and J. A. Dumesic.

Density Functional Theory and Reaction Kinetics Studies of the Water Gas Shift Reaction on PtRe Catalysts, accepted in *Heterogeneous, Homogeneous, Bio- and Nano-catalysis (ChemCatChem)*, Ronald Carrasquillo-Flores, Jean Marcel R. Gallo, Konstanze Hahn, Manos Mavrikakis, and J. A. Dumesic.

Synthesis and evaluation of an integrated strategy for the catalytic conversion of hemicellulose and cellulose from lignocellulosic biomass to liquid transportation fuels, accepted in *Green Chemistry*, Jeehoon Han, S. Murat Sen, David Martin Alonso, Christos T. Maravelias, and J. A. Dumesic.

Bimetallic RhRe/C catalysts for the production of biomass-derived chemicals, accepted in the *Journal of Catalysis*, Mei Chia, Brandon J. O'Neill, Ricardo Alamillo, Paul J. Dietrich, Fabio H. Ribeiro, Jeffrey T. Miller, and J. A. Dumesic.

Stabilization by Atomic Layer Deposition of Cu Catalysts for Liquid-Phase Reactions, accepted in *Angewandte Chemie International Edition*, Brandon J. O'Neill, David H. K. Jackson, Anthony J. Crisci, Carrie A. Farberow, Fengyuan Shi, Ana C. Alba-Rubio, Junling Lu, Paul J. Dietrich, Xiangkui Gu,Christopher L. Marshall, Peter C. Stair, Jeffrey W. Elam, Jeffrey T. Miller, Fabio H. Ribeiro, Paul M. Voyles, Jeffrey Greeley, Manos Mavrikakis, Susannah L. Scott, Thomas F. Kuech, and James A. Dumesic

Sole funding by other agencies:

Techno-economic analysis of dimethylfuran (DMF) and hydroxymethylfurfural (HMF) production from pure fructose in catalytic processes, *Chemical Engineering Journal* **169**, 329 (2011), Akshay Patel, Juan Carlos Serrano-Ruiz, Robert P. Anex, and J. A. Dumesic.

Improved Hydrothermal Stability of Niobia-Supported Pd Catalysts, *Applied Catalysis A: General* **397**, 153 (2011), Hien N. Pham, Yomaira J. Pagan-Torres, Juan Carlos Serrano-Ruiz, Dong Wang, Abhaya K. Datye, and J. A. Dumesic.

Selective hydrogenolysis of polyols and cyclic ethers over bifunctional surface sites on rhodium-rhenium catalysts, *Journal of the American Chemical Society* **133**, 12675 (2011), Mei Chia, Yomaira J. Pagán-Torres, David Hibbitts, Qiaohua Tan, Hien N. Pham, Abhaya K. Datye, Matthew Neurock, Robert J. Davis, and J. A. Dumesic.

Production of Biofuels from Cellulose and Corn Stover Using Alkylphenol Solvents, *Chemistry and Sustainability* **4**, 1078 (2011), David Martin Alonso, Stephanie G. Wettstein, Jesse Q. Bond, Thatcher W. Root, and J. A. Dumesic.

Liquid-phase catalytic transfer hydrogenation and cyclization of levulinic acid and its esters to γ-valerolactone over metal oxide catalysts, *Chemical Communications* **47(44),** 12233 (2011), Mei Chia, and J. A. Dumesic.

Production of 5-Hydroxymethylfurfural from Glucose Using a Combination of Lewis and Brønsted Acid Catalysts in Water in a Biphasic Reactor with an Alkylphenol Solvent, *ACS Catalysis* **2**, 930 (2012), Yomaira J. Pagán-Torres, Tianfu Wang, Jean Marcel R. Gallo, Brent H. Shanks, and J. A. Dumesic.

Water-compatible Lewis acid-catalyzed conversion of carbohydrates to 5-hydroxymethylfurfural in a biphasic solvent system, *Topics in Catalysis* **55**, 657 (2012), Tianfu Wang, Yomaira J. Pagán-Torres, Elliot J. Combs, Brent H. Shanks, and J. A. Dumesic.

The selective hydrogenation of biomass-derived 5-hydroxymethylfurfural using heterogeneous catalysts, *Green Chemistry* **14**, 1413 (2012), Ricardo Alamillo, Mark Tucker, Mei Chia, Yomaira Pagán-Torres, and J. A. Dumesic.

Acid-Functionalized SBA-15-Type Periodic Mesoporous Organosilicas and their Use in the Continuous Production of 5-Hydroxymethylfurfural, *ACS Catalysis* **2**, 1865 (2012), Mark H. Tucker, Anthony J. Crisci, Bethany Wigington, Neelay Phadke, Ricardo Alamillo, Jinping Zhang, Susannah L. Scott, and J. A. Dumesic.

Triacetic Acid Lactone as a Biorenewable Platform Chemical, *Green Chemistry* **14**, 1850 (2012), Mei Chia, Thomas J. Schwartz, Brent H. Shanks, and J. A. Dumesic.

Ce promoted Pd-Nb catalysts for γ-Valerolactone ring-opening and hydrogenation, *Green Chemistry* **14**, 3318 (2012), R. Buitrago, J.C. Serrano-Ruiz, A. Sepúlveda-Escribano, F. Rodríguez-Reinoso, and J. A. Dumesic.

Sn-beta catalysed conversion of hemicellulosic sugars, *Green Chemistry* **14**, 702 (2012), M.S. Holm, Y. J. Pagan-Torres, S. Saravanamurugan S, A. Riisager, E. Taarning, and J. A. Dumesic.

Influence of Alkali and Alkaline Earth Metal Salts on Glucose Conversion to 5-Hydroxymethylfurfural in an Aqueous System, *Catalysis Communications* **30**, 1 (2013), Elliot Combs, Basak Cinlar, Yomaira Pagan-Torres, Brent H. Shanks, and J. A. Dumesic.

Catalysis with ceria nanocrystals: bio-oil model compound ketonization, *Applied Catalysis A: General* **464-465**, 288 (2013), Ryan W. Snell, Sikander H. Hakim, Brent H. Shanks, and J. A. Dumesic.

Sustainable solvent systems for use in tandem carbohydrate dehydration-hydrogenation, *ACS Sustainable Chemistry & Engineering* **1**, 554 (2013), Mark H. Tucker, Ricardo Alamillo, Anthony J. Crisci, Gretchen M. Gonzalez, Susannah L. Scott, and J. A. Dumesic.

Mechanistic Insights into Ring-Opening and Decarboxylation of 2-Pyrones in Liquid Water and Tetrahydrofuran, *Journal of the American Chemical Society* **135**, 5699 (2013), Mei Chia, M. Ali Haider, Gerald Pollock III, George A. Kraus, Matthew Neurock, and J. A. Dumesic.

Mechanocatalytic depolymerization of (ligno)cellulose as an entry-process for high-yield production of HMF and furfural in a biphasic system, *ACS Catalysis* **3**, 993 (2013), Ronald Carrasquillo-Flores, Mats Käldström, Ferdi Schüth, Roberto Rinaldi, and J. A. Dumesic.

Tailored Microenvironments for Catalytic Biomass Conversion in Inorganic-Organic Nanoreactors, *Angewandte Chemie International Edition* **52**, 10349 (2013), Anthony J. Crisci, Ricardo Alamillo, Jean Marcel Gallo, Susannah L. Scott, and J. A. Dumesic.

Integration of chemical and biological catalysis: production of furylglycolic acid from glucose via cortalcerone, accepted in *ACS Catalysis*, Thomas J. Schwartz, Samuel M. Goodman, Christian Osmundsen, Esben Taarning, Michael D. Mozuch, Jill Gaskell, Daniel Cullen, Philip J. Kersten, and J. A. Dumesic.

Grant Number	Invention Title	Inventors		Date Fed Government Notified	UW Log #/WARF P#
144 HE11 9802238 DE-FG02-84ER13183	low temperature hydrogen production from oxygenated hydrocarbon	Randy James	Cortright Dumesic	May 21, 2004	1556 / P01411US
144 GJ89 DE-FG02-84ER13183	low temperature catalytic process to produce hydrocarbons from sugars	Randy James	Cortright Dumesic	January 07, 2002	1669 / P02136US
144 GJ89 DE-FG02-84ER13183	Low-temperature hydrogen production from oxygenated hydrocarbons	Randy James	Cortright Dumesic	July 24, 2002	1833 / P02346US

Grant Number	Invention Title	Inventors		Date Fed Government Notified	UW Log #/WARF P#
144 GJ89 DE-FG02-84ER13183	Catalytic reforming of oxygenated hydrocarbons combined with ultra-shift for hydrogen with very low levels of carbon monoxide	Rupali James	Davda Dumesic	May 28, 2003	2087 / P03305US
144 GJ89 DE-FG02-84ER13183	Room temperature process for the selective oxidation of carbon monoxide in hydrogen gas streams for proton exchange membrane fuel cells	James Won Gabriel Tobias	Dumesic Kim Rodriguez Rivera Voitl	June 21, 2004	2440 / P04360US
144 MH43 0327959 DE-FG02-84ER13183	Stable Aqueous-Phase Basic Catalysts	James George Juben Christopher	Dumesic Huber Chheda Barrett	September 20, 2005	2864 / P06037US